Prominence of the Instability of a Stabilizing Agent in the Changes in Physical State of a Hybrid Nanomaterial

Gregory Spataro, Yohan Champouret, Yannick Coppel, Myrtil L. Kahn

Prominence of the instability of a stabilizing agent in the changes in physical state of a hybrid nanomaterial

Grégory Spataro,[a]‡ Yohan Champouret,[a]‡ Yannick Coppel,[a]* and Myrtil L. Kahn[a]*

[a]Drs. G. Spataro, Y. Champouret, Y. Coppel, and M. L. Kahn

Laboratoire de Chimie de Coordination

CNRS UPR 8241,University of Toulouse, 205 route de Narbonne, 31077 Toulouse (France)

E-mail: yannick.coppel@lcc-toulouse.fr; myrtil.kahn@lcc-toulouse.fr

‡These authors contributed equally.

Abstract: Shaping ability of hybrid nanomaterials is a key point for their further use in devices. It is therefore crucial to control it. To this end, it is necessary that the macroscopic properties of the material remain constant over time. Here, we evidence by multinuclear Magic-Angle Spinning Nuclear Magnetic Resonance spectroscopic study including ^{17}O isotope exchange that for a ZnO-alkylamine hybrid material, the partial carbonation of amine into ammonium carbamate molecules is behind the conversion from highly viscous liquid to a powdery solid when exposed to air. This carbonation induces modification and reorganization of the organic shell around the nanocrystals and affects significantly the macroscopic properties of the material such as it physical state, its solubility and colloidal stability. This study, straightforwardly extendable, highlights that the nature of the functional chemical group allowing connecting the stabilizing agent (SA) to the surface of the nanoparticles is of tremendous importance especially if the SA is reactive with molecules present in the environment.

Introduction

Stabilizing agents (SAs) used for the preparation of nanoparticles in solution are of tremendous importance for the control of their size and shape[1-7] as well as for their colloidal stability.[8-11] Their role on the nanomaterial's properties is also established for magnetic,[8, 12] optical,[13-15] thermoelectric,[16] catalytic properties,[17-21] and biocompatibility.[22-24] However, so far, their role on the physical state of bulk hybrid organic-inorganic materials (*i.e.* liquid, viscous, solid…) has been hardly considered while this physical state is of tremendous importance for nanomaterial shaping.

A typical SA possesses a functional chemical group allowing its linkage to the surface of the nanoparticles. The nature of this functional chemical group is found to vary from one nanoparticle's preparation to another but primary alkylamines are among the most commonly used SAs.[25-28] However, amines are not inert molecules in ambient conditions. They are known to quickly form alkyl ammonium-alkyl carbamate (AmCa) when exposed to CO_2[29-30] and are long been used for the capture of carbon dioxide from various sources.[31-33] The formation of AmCa ion pairs is well documented for various systems and is used as organogelator,[34] for nanocrystal synthesis,[35-36] and for controlling self-assembly.[37-39]

Herein, we evidence that the change of the physical state of ZnO-alkylamine hybrid material when exposed to air is due to the partial carbonation of the alkylamine into AmCa species. In turn, this carbonation induces a strong modification and reorganization of the organic shell around the nanocrystals.

Before exposure to air, alkylamines are the only SAs at the surface of the nanocrystals. They are bent with a high population of disordered gauche conformers and present notable local motions that limit

their stacking yielding a viscous material. When exposed to air, AmCa molecules start to form. These adopt a rigid all-trans conformation at the surface of the nanocrystals and the hybrid nanomaterial turns into a powdery product. These conclusions are based on multinuclear ^{13}C, ^{15}N, and ^{17}O MAS NMR spectroscopic studies. Change in the colloidal stability of the material is also discussed based on the liquid state NMR experiments.

Results and Discussion

ZnO nanocrystals (NCs) were synthesized following a procedure reported by our group.[40] This approach consists in the controlled hydrolysis of the dicyclohexyl zinc compound, $[Zn(Cy)_2]$, in presence of dodecylamine (DDA) (see experimental part for details). Typically, the precursor was dissolved in a THF solution containing DDA and a THF solution with 2 equivalents of water (or ^{17}O-enriched H_2O, *vide infra*) was added dropwise. Well-defined isotropic ZnO NCs of around 8.0 (1.0) nm (see Figure S1) are produce quantitatively after stirring under argon for 16 h.

Surprisingly, while individually DDA and ZnO are powders, the resulting product (hereafter ZnO@DDA) is an oily-viscous material. However, it evolves to a powdery solid in a short time (typically 24 h) when exposed to air. The viscous state is very advantageous for shaping but its change with time into powder is damaging. It is therefore of prime importance to understand the chemical and physical-chemical processes behind these observations. This was made possible by revisiting our previous results[41] and comparing them with those obtained when the material is exposed to air.

The most likely origin for this change in physical state is the hybrid interface. Therefore, in order to probe the transformations taking place at the SA level, NMR appeared to be the most suitable technique. Solid state NMR spectroscopy is nowadays a well-established tool for studying inorganic nanoparticles.[42-46] Whether these latter are metallic, metal oxides or semiconducting, NMR allow to disclose information of prime importance regarding the structural and dynamic characterization of the SAs on their surface as well as the nanoparticles themselves.[47-51] For example, identification of facet-dependent coordination mode of SAs on nanocrystals,[51] description of the chemical environment of the metallic site at the surface or in the core of the nanoparticles,[43] and the impact of anchored anionic SAs on the chemical stability of nanoparticles have been recently deciphered.[49] NMR spectroscopy can therefore meet challenges in nanoscience.

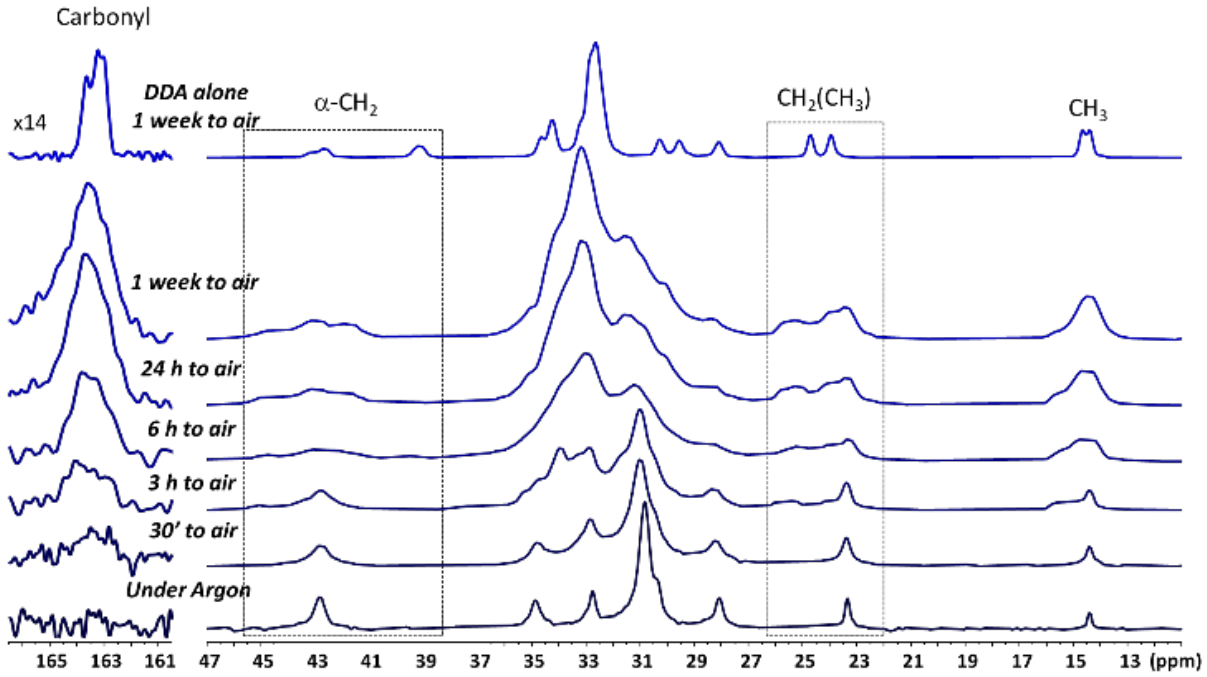

Figure 1. ^{13}C CP MAS spectra of ZnO@DDA prepared under argon atmosphere when exposed to air over time. The intensity of the left part of the spectra is increased 14 times to better evidence the carbamate carbonyl signal. ^{13}C CP MAS spectrum of DDA molecules exposed to water vapor-saturated air for one week (AmCa) is provided as a reference.

Prior to exposure to the air, ^{13}C MAS NMR spectra of ZnO@DDA show that both rigid and mobile DDA are present in this hybrid material (see SI for details). All the DDA ^{13}C resonances are indeed observed regardless of the polarization transfer sequence (Figures 1 and 2). Rigid DDA are edited with Cross-Polarization (CP, Figure 1 bottom spectrum); these are molecules interacting with the ZnO surface. They correspond to the first SA shell (pale blue in Scheme 1). Mobile DDA are edited with INEPT sequence (Figure 2 bottom spectrum), and correspond to molecules located further from the surface. These DDA form the second SA shell (deep blue in Scheme 1). The populations between rigid and mobile DDA was determined using the distinct chemical-shift of their respective C atom in gamma position with respect to the amine function in the MAS spectrum with direct polarization (DP, Figure S2). The rigid/mobile population was found to 70/30 (±5) for ZnO NCs prepared with 0.2 eq. of DDA. In addition, the alkyl chain of DDA in the first SA shell exhibits a bent structure with trans-gauche or gauche-gauche configuration (the central methylene groups of DDA are observed at 31.0/30.0 ppm,[52] Figures 1 and 2 bottom spectra) associated with weak hydrogen bonds between β and/or γ-CH_2 and the ZnO surface (Figure S3). Furthermore, ^{15}N MAS spectrum (Figure 3) exhibits only one resonance at - 356 ppm. The coordination of DDA onto the ZnO surface is a Lewis-like mode with O-Zn···N dative bonds (Figure 3 bottom spectrum). All these results allow understanding the oily-viscous state of ZnO@DDA. It results from the bent DDA that are coordinated to the ZnO surface. These DDA located in the first SA shell albeit relatively rigid (they are observed with ^{13}C CPMAS experiment) show significant local motions that hinder stacking by Van der Waals interactions. This hybrid interface, with its unique mode of amine coordination on the NC's surface, affects the second SA shell. Indeed, the stacking of SAs by Van der Waals interactions being hindered, this leads to the presence of highly mobile DDA in the second SA shell that behave as liquid molecules; as a result the product is oily-viscous (Scheme 1).

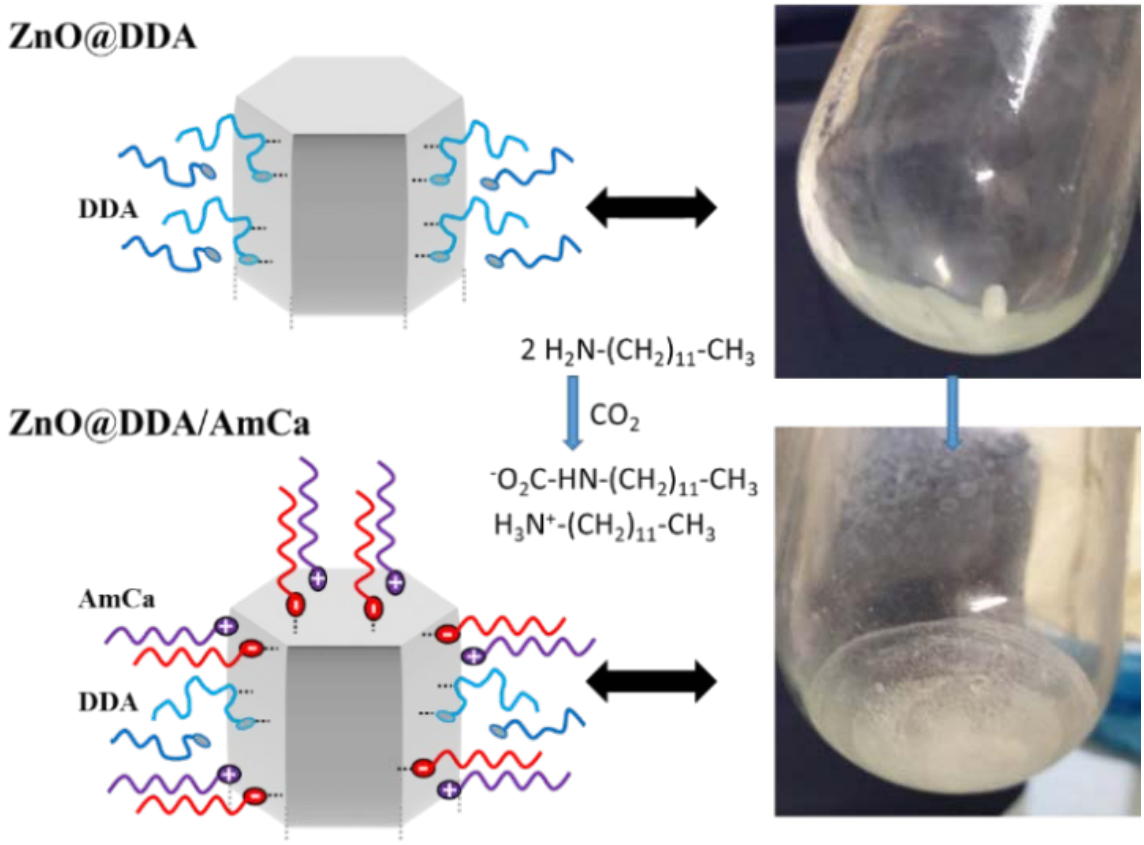

Scheme 1. Overview of the proposed model for the transformation of ZnO@DDA to ZnO@DDA/AmCa over the time of air exposure. The hybrid material evolves from an oily-viscous product to a powdery solid.

Over the time of air exposure, the ^{13}C CP MAS signals become more and more intense (Figure 1 and S4) while concomitantly, the reverse is observed for ^{13}C INEPT MAS signals (Figure 2). The population of mobile SAs strongly decreases in favor of rigid ones. Up to 24 h of air exposure, the ^{13}C CP MAS spectra show notable modification for all the DDA resonances that become broader, while after this time, only very small changes are noticeable. Such spectrum is characteristic of an organic shell with a significant structural heterogeneity. New signals at ~163.5, ~45, and 25/26 ppm associated respectively to carbonyl group, α-CH_2, and $CH_2(CH_3)$ carbons of carbamate species are observed. These chemical shifts are significantly deshielded and broader in the presence of ZnO NCs compared to the ones of AmCa alone (Figure 1 top), suggesting interaction of AmCa species with ZnO NCs. Over time, other signals appeared at 41.8 ppm and 23.8/23.2 ppm respectively for α-CH_2 and $CH_2(CH_3)$, that confirm the significant structural heterogeneity of the organic shell surrounding the ZnO NCs (Figure S4).

Concomitantly to the appearance of the above mentioned signals, the signal associated to central methylene carbons (in the 30-34 ppm range) evolved from a signal centered around 31 / 30 ppm for ZnO@DDA, characteristic of methylene groups with trans-gauche or gauche-gauche conformations, to a signal centered around 33 / 34 ppm, characteristic of methylene groups with all-trans conformations.

Remarkably though, after a week of air exposure, residual amine signals are still observed (notably the α-CH_2 carbons at ~28.1 ppm, Figure S4). The initial system of alkylamine-stabilized ZnO NCs has evolved

into a system of ZnO NCs stabilized by both alkylamine and AmCa species. Evaluation of the proportion of one to the other of these two species was not possible with ^{13}C spectra because of strong signal overlaps, but this information was obtained from ^{15}N MAS NMR data (see below).

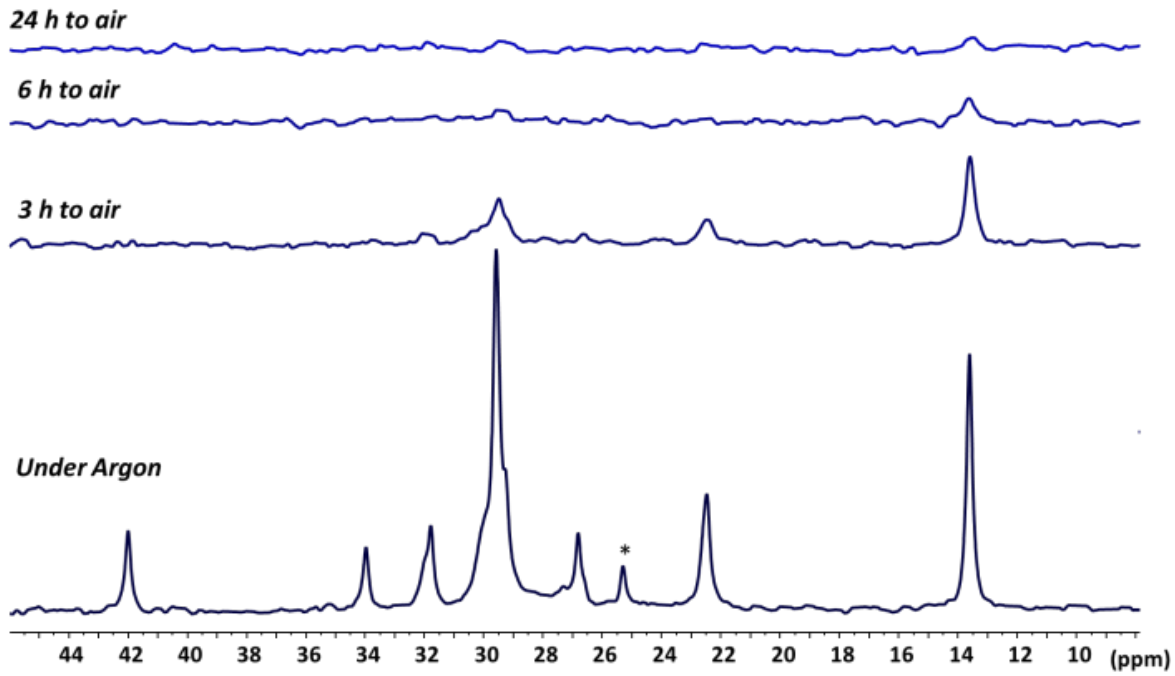

Figure 2. ^{13}C INEPT MAS spectra of ZnO@DDA prepared under argon atmosphere and then exposed to air for different time periods.*: THF.

Dynamics of these molecules at the surface of the ZnO NCs were evaluated by measuring the dipolar couplings of C-H pairs (D_{CH}) using Magic-Echo CP (ME-CP) experiments (Figure S6).[53] Despite the complexity of the ME-CP spectrum, D_{CH} values of 21, 13, and 2 kHz have been evidenced, which correspond to rigid, semi-rigid, and mobile CH_2 species, respectively.[53] Note that values of 2 kHz have been previously measured for ZnO@DDA and are characteristic of a notable mobility of the chains.[41] This confirms that some bent DDA with a trans-gauche or gauche-gauche configuration are still present at the ZnO surface all over the time. D_{CH} values of 21 and 13 kHz can tentatively be assigned to respectively rigid carbamate species directly coordinated to the ZnO surface and more mobile ammonium species electrostatically associated to the surface, as suggested theoretically,[54] and observed experimentally here for the first time.

The ^{15}N CP MAS experiments strengthen and complete the above described surface state of the ZnO NCs. ^{15}N CP MAS spectrum of ZnO@DDA under argon exhibits only one signal at -355.8 ppm (Figures 3 bottom). Over time of air exposure, this signal becomes weaker and more complex, in agreement with a significant structural heterogeneity. Concomitantly, two set of signals at -297.4/-298.2 and -359.7/-360.9 ppm corresponding respectively to the carbamate (Ca^-) and ammonium (Am^+) species emerge.[36] They become predominant after 1 week of air exposure. Compared to the signal of AmCa alone (Figure 3 top), the ^{15}N AmCa signals are shifted (ca. 225 Hz and 585 Hz for the signals at -292.3 ppm and -345.9 ppm, respectively) in the presence of ZnO NCs which confirms the interaction of AmCa with the NCs. Integration of the ^{15}N signals makes it possible to roughly estimate the presence of one residual DDA for four AmCa molecules. This corresponds to about 10% of the remaining DDA molecules (Figure S7).

This corresponds to an approximate value as the reliability of the quantification were not evaluated (CP intensities depend of local hydrogen densities and dynamics).

It is noteworthy that the two set of signals for Ca^- and Am^+ in the presence of ZnO NCs reveals that AmCa is located in two different surface environments. Integration of the ^{15}N resonances yields a proportion of about 40/60±10 of these localizations (Figure S7), a ratio similar to that between lateral and basal faces (*i.e.* 46/53, see SI for details) of a ZnO NC. Even if the reliability of the quantification is not guaranteed, we believe that the intensity difference for these two signals, associated to two very similar AmCa species, is sufficient to tentatively assign them to AmCa bound on the basal and lateral faces, respectively. In the following, the ZnO sample stabilized by both DDA and AmCa will be called ZnO@DDA/AmCa.

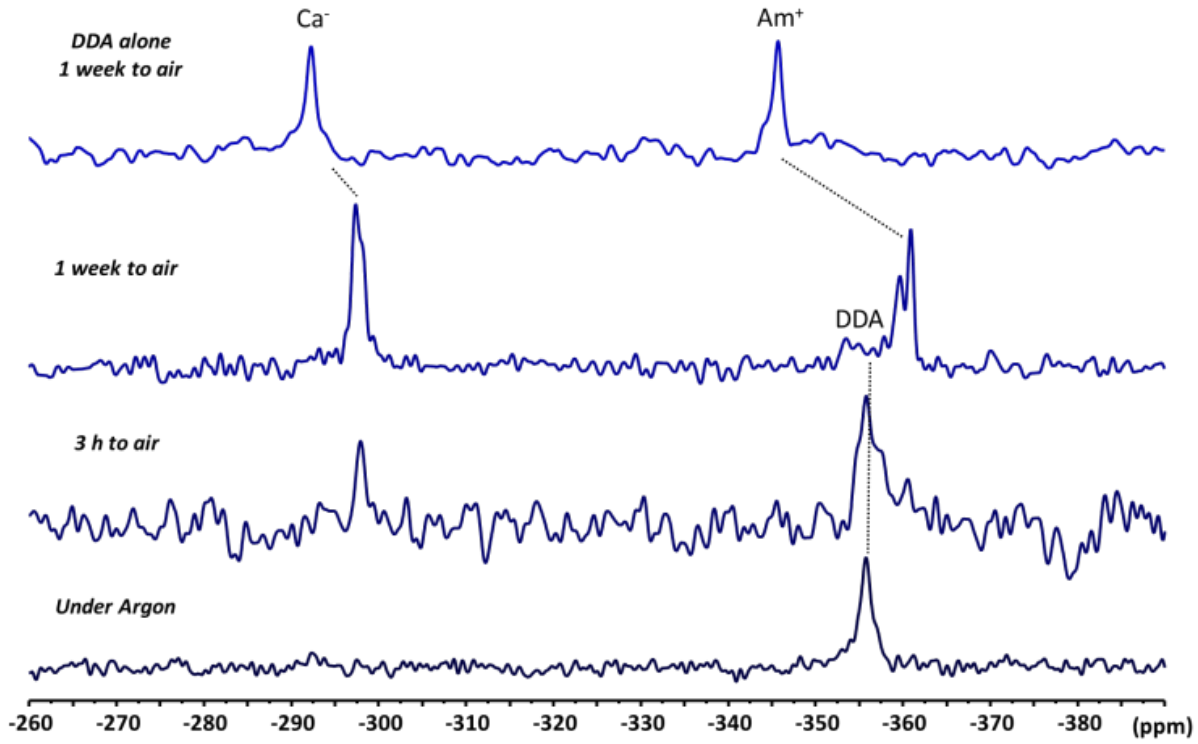

Figure 3. ^{15}N CP MAS spectra of ZnO@DDA, ZnO@DDA/AmCa after 3h and 1 week of air exposure, and AmCa.

The changes of the DDA signal observed for ZnO@DDA/AmCa are a proof that some AmCa molecules are located on the lateral faces since we have previously shown that in ZnO@DDA the DDAs are located only on these faces.[41, 54] The presence of carbamate molecules on the basal faces of the ZnO NCs was definitely proven by ^{17}O isotope exchange using ^{17}O-enriched water. For this experiment, ZnO@DDA/AmCa was prepared by exposing ZnO@DDA only to CO_2 for 3 days. Formation of AmCa was confirms by ^{13}C CP MAS measurement (Figure S8). After exposition to ^{17}O-enriched water 1D T_1-filtered ^{17}O MAS NMR spectra at 9.4 T were recorded as a function of time for both ZnO@DDA/AmCa and ZnO@DDA (Figure S9-S10). Three main ^{17}O signal areas centered at -17.8, -23.2, and -29.2 ppm are observed regardless of the sample (Figure S11). The exchange rates, k_{glo}, were obtained by monitoring the changes of the peaks integral for the three ^{17}O ZnO resonances over time (Figure 4). For ZnO@DDA/AmCa, k_{glo} is equal to 0.07 h^{-1}, a value about 15 times lower than for ZnO@DDA (k_{glo} = 1.08

h^{-1}). The final Isotope Enrichment Level (IEL) that is a standardized value (^{17}O signal integral per milligram of sample) characteristic of the equilibrium state in the isotope exchanges (*i.e.* the plateau values), is about 3 times smaller for ZnO@DDA/AmCa than for ZnO@DDA (IEL = 100, and IEL = 290, respectively). Moreover, the ^{17}O spectra at the equilibrium state of the exchange experiment of ZnO@DDA/AmCa and ZnO@DDA are slightly different (Figure S12). In particular, the ratio between the high and low frequencies ^{17}O signals (*i.e.* -17.9 ppm area / -23.2 to -29.2 ppm areas) is equal to ~ 70/30 and ~ 80/20 for ZnO@DDA/AmCa and ZnO@DDA, respectively. These results demonstrate that, when AmCa is present 1) the ^{17}O isotope exchange rate is slowed down, 2) the amount of exchangeable oxygen atoms is reduced, and 3) the proportion of exchangeable oxygen atoms in the core of the ZnO NCs decreased. Those results clearly evidence a reduced accessibility for H_2O to ZnO for ZnO@DDA/AmCa compared to ZnO@DDA. The water diffusion to the lateral faces may also be hindered by the stacking of the AmCa moieties. However, since ligands in ZnO@DDA already are hydrophobic it should hardly change the diffusion rate. More likely, these results can be explained by the coordination of AmCa molecules at the basal faces of the NCs since we have previously shown that for ZnO@DDA, the diffusion of oxygen atoms inside the NCs takes place through the basal faces, which are originally free of any ligands (Scheme 1).[48]

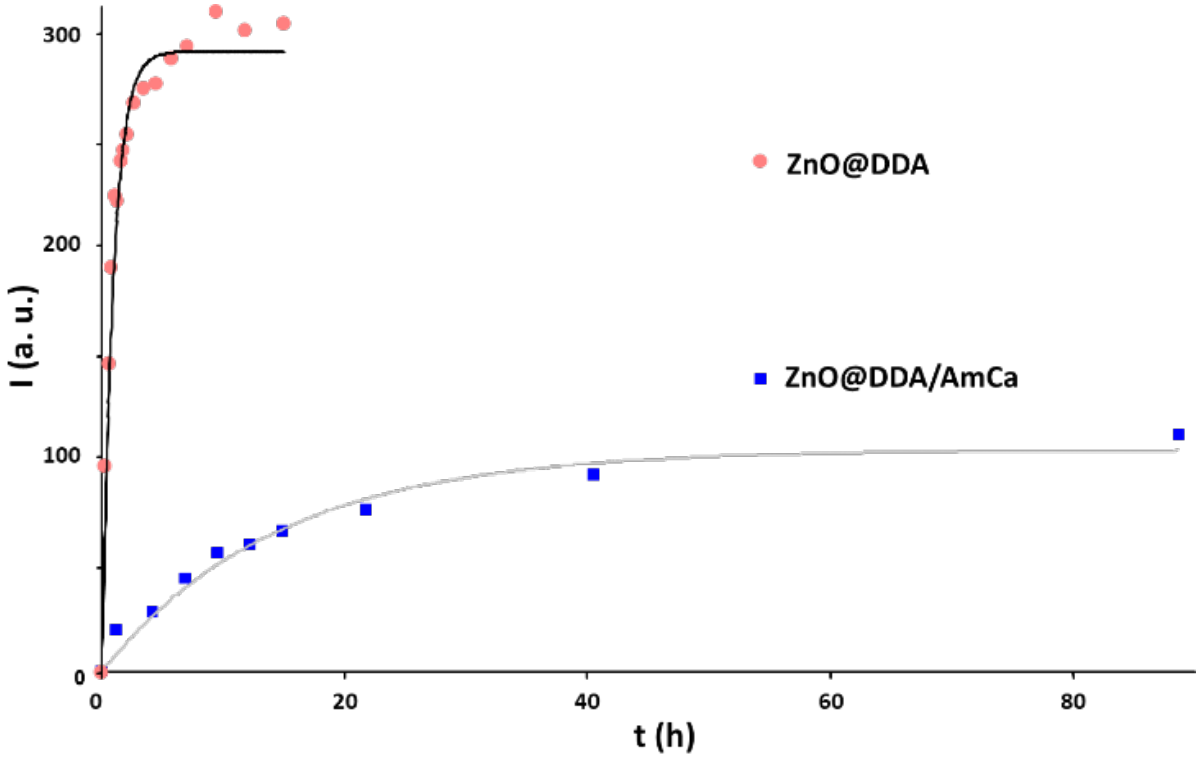

Figure 4. ^{17}O signal integral (standardized according to sample mass) of ZnO@DDA/AmCa (blue squares) and ZnO@DDA (0.2 eq. DDA) (red dots) as a function of the contact time to enriched H_2O. Fitting is obtained using the equation: $I(t) = I(\infty)[1 - \exp\{-k.t\}]$.

These results allow drawing a realistic mechanism. After adsorption of CO_2 molecules onto the ZnO surface, CO_2 can chemisorb or react with physisorbed H_2O molecules that are already present after the ZnO synthesis or that come from the atmosphere. This reaction could generate reactive HCO_3^- and H_2CO_3 species onto the ZnO surface.[55] Then, by diffusion, DDA come into contact to those species,

react, which leads to the formation of the AmCa bounded to the surface (notably on the basal faces). As the mobile DDA diffuse probably much faster than the rigid ones, they are transformed in AmCa first. The rigid DDA that are in a direct interaction with the ZnO NC also has some mobility and can react as well. At the end, the presence of residual strongly bound rigid DDA molecules can be probably explained by a densification and a rigidification of the organic layer surrounding the ZnO NC over time that trap these DDA molecules.

Consequence on the shaping ability of the material: While ZnO@DDA is a very stable colloid, ZnO@DDA/AmCa's solubility and stability are much lower, which is dramatic for the shaping of this material by inkjet process, for example. With the above described MAS NMR results in mind, liquid state ^{1}H NMR experiments have provided further insights in the reasons for this loss of colloidal stability when AmCa is present on the surface of NCs. For all NMR experiments (1D ^{1}H (Figure S13), DOSY and diffusion-filtered ^{1}H (Figure S14), and NOESY (Figure S15)) sharper resonances are observed for ZnO@DDA/AmCa as compared to ZnO@DDA. These resonances correspond only to signals from the DDA in weak interaction with ZnO NCs;[56] no signal for free or weakly bound AmCa are detected (Figure S13). This indicates a strong chemical affinity of AmCa molecules for the ZnO's surface. Strongly bonded molecules present indeed a reduced mobility that leads to the disappearance or the strong broadening of their NMR signals due to fast T_2 relaxation. Moreover, a faster average diffusion coefficient is measured for the weakly bound DDA molecules in ZnO@DDA/AmCa compared to ZnO@DDA (respectively 11.1(±0.2) x 10^{-10} and 9.7(±0.3) x 10^{-10} $m^2.s^{-1}$, Figure S14), which substantiates a higher release of DDA from the NCs' surface in the presence of AmCa species (see SI for details). Additionally, slow diffusion coefficients of 0.6 (±0.1) x 10^{-10} and 0.2 (±0.1) x 10^{-10} $m^2.s^{-1}$ (Figure S14) associated to the strongly bonded SAs could be measured for ZnO@DDA and ZnO@DDA/AmCa, respectively. The first values is in agreement with the expected ZnO NCs' hydrodynamic diameter – calculated using the Stokes-Einstein equation - of 12(□ 2) nm (ZnO NC of 8 nm, measured from TEM, plus the organic layer) while the second values corresponds to a hydrodynamic diameter of 35(□ 10) nm, a diameter too large for isolated NCs but characteristic of aggregation.

The formation of aggregates is likely due to electrostatic interactions between charged molecules,[39] such as AmCa, but a deeper modification of the organic shell can also contribute to it. The organic surroundings of ZnO@DDA is a multilayer made of DDA in equilibrium with free DDA in solution.[56] The carbonation of the amines leads to the substitution of DDA by AmCa that has a stronger chemical affinity for ZnO's NCs. No dynamic exchange between AmCa molecules on the surface of the NCs and free molecules in solution is observed. Furthermore, the conformation of the alkyl chains changes from a trans-gauche to an all-trans conformation; the ideal conformation for compact stacking. Intermingling of extended alkyl chains become favorable. The entire organic layer becomes rigid. The amines remaining on the surface and which can still exchange with those in solution (transferred NOEs are observed for DDA, Figure S15) are in too small quantities to ensure the colloidal stability of the system (ca. 10% from solid state NMR studies, see above). This leads ZnO@DDA/AmCa to aggregate and finally flocculate. This model is confirmed by the diffusion-filtered ^{1}H signal of the slow diffusing species ZnO@DDA/AmCa, showing only one very broad signal centered at 1.75 ppm corresponding to the central methylene groups. The broadness of this signal associated with the absence of the signal of terminal methyl group confirm the rigidity of the entire alkyl chains at the surface of ZnO@DDA/AmCa. Note that the results reported here are independent of the size and shape of the starting ZnO@DDA NCs.

Conclusion

The gathered results show that technological problems such as the modification over time of the physical state of a hybrid material can find their origin at the molecular level. We have shown this for ZnO nanoparticles stabilized by alkylamine, a very widespread SA. Our observations and conclusions may therefore be straightforwardly extended towards many amine-based hybrid systems. Other stabilizing agents may also be reactive with their environment, and more systematic studies of these phenomena would certainly provide a better grasp and understanding of the aging of hybrid organic-inorganic nanomaterials.

Experimental Section

Materials. All reactions were carried out under an oxygen-free argon atmosphere using standard Schlenk and glovebox techniques. Tetrahydrofuran (THF) was dried using an MBraun SPS column. The residual water contents of the solvent were systematically measured by Karl Fischer coulometric titration by using Metrohm equipment. $Zn(C_6H_{11})_2$ was purchased from NanoMePS. Dodecylamine (DDA) was purchased from Aldrich and used as received in the glove box. H_2O was distilled under argon and degassed by bubbling argon for 30 min. D_2O (99.90% D) and H_2O-enriched ^{17}O (20% ^{17}O) were purchased from Euriso-top and degassed by bubbling argon for at least 30 min.

Synthesis. *Preparation of Sample ZnO@DDA:* In a dry Schlenk, $Zn(C_6H_{11})_2$ (348 mg, 1.5 mmol) and dodecylamine (55.6 mg, 0.2 equiv., 0.3 mmol) were dissolved in 17 mL of THF and vigorously stirred at room temperature for 5 min protected from light. 0.69 mL of wet THF containing H_2O (2 equiv., 3 mmol) was then added dropwise to the $Zn(C_6H_{11})_2$/DDA mixture. After 16 h, the solvent was removed under vacuum to quantitatively yield ZnO NCs. Preparation of Sample ZnO@DDA/AmCa for ^{17}O isotopic exchange experiment and liquid state NMR: Sample ZnO@AmCa is prepared by exposing Sample ZnO@DDA to CO_2 gas in a glovebox (Fisher-Porter reactor) for 3 days.

Sample preparation for ^{17}O isotope exchange experiments: Under argon, 20 μL of degassed H_2O-enriched with ^{17}O (20% ^{17}O) was added directly inside the zirconia rotor containing 20 mg of ZnO@DDA or 30 mg of ZnO@DDA/AmCa.

Characterization. *Transmission Electron Microscopy*: Samples for TEM analysis were prepared by slow evaporation of droplets of colloidal THF solution deposited on carbon-supported copper grids. The samples were dried overnight under vacuum (1×10^{-5} mbar) by using a BOC Edward turbomolecular pump. The TEM experiments were recorded at the "Service Commun de Microscopies de l'Université Paul Sabatier" TEMSCAN on a JEOL JEM1011 electron microscope operating at 100 kV. The nanoparticle size-distribution histograms were determined by using magnified TEM images. The size-distribution of the particles was determined by measuring a minimum of 250 particles for each sample. The size-distributions were generally analyzed in terms of Gaussian statistics. *Solid-state NMR* experiments were recorded on Bruker Avance III spectrometers operating at magnetic fields of 9.4 T. Samples were packed into 3.2 mm zirconia rotors inside a glovebox. Note that the MAS rotors are sufficiently airtight to protect samples. The rotors were spun at 8 or 12 kHz at 293K. ^{13}C CP and ^{15}N CP MAS spectra were recorded with a recycle delay of 2 s and contact times of 2 ms and 3 ms, respectively.^{13}C INEPT was recorded with a recycle delay of 3 s. 2D ME-CP spectra were recorded with a RF field strength of 90 kHz for ^{1}H and 102/78 kHz for ^{13}C during the dipolar evolution. 1D *T_1-filtered* ^{17}O MAS experiments were acquired with a time delay t_{filter} of 40 ms and with a recycle time of 2 s to follow the isotope exchange kinetics and of 20 s for quantification purposes (relative population and isotopic enrichment level).[48] Chemical shifts were referenced to liquid TMS, water, CH_3NO_2, ^{13}C, ^{17}O

and ^{15}N, respectively. All spectra were fitted using the DMfit software.[57] 1D and 2D ^{1}H liquid state NMR experiments were recorded on a Bruker Avance NEO 600 spectrometer equipped with a 5 mm triple resonance inverse Z-gradient probe. Samples were prepared in toluene-d_8. The 2D NOESY measurements were done with a mixing time of 100 ms. DOSY measurements were made using the stimulated echo pulse sequence with bipolar gradient pulses. The diffusion dimension was processed with the Laplace inversion routine CONTIN (Topspin software).

Acknowledgements

This work was supported by both the Centre National de la Recherche Scientifique (CNRS) and by the French National Agency (ANR) as part of its program in Nanosciences and Nanotechnologies (EVALON project no. ANR-08-NANO-026).

Keywords: hybrid materials • surface chemistry • NMR spectroscopy • properties • nanoparticles

[1] J. D. Smith, C. M. Bunch, Y. Li, K. M. Koczkur, S. E. Skrabalak, *Nanoscale* **2019,** *11* (2), 512-519.
[2] N. S. R. Satyavolu, K. Y. Loh, L. H. Tan, Y. Lu, *Small* **2019**, e1900975-e1900975.
[3] A. Heuer-Jungemann, N. Feliu, I. Bakaimi, M. Hamaly, A. Alkilany, I. Chakraborty, A. Masood, M. F. Casula, A. Kostopoulou, E. Oh, K. Susumu, M. H. Stewart, I. L. Medintz, E. Stratakis, W. J. Parak, A. G. Kanaras, *Chem. Rev.* **2019,** *119* (8), 4819-4880.
[4] M. Rambukwella, N. A. Sakthivel, J. H. Delcamp, L. Sementa, A. Fortunelli, A. Dass, *Front. Chem.* **2018,** *6*, 330.
[5] S. Lu, H. Yu, S. Gottheim, H. Gao, C. J. DeSantis, B. D. Clark, J. Yang, C. R. Jacobson, Z. Lu, P. Nordlander, N. J. Halas, K. Liu, *J. Am. Chem. Soc.* **2018,** *140* (45), 15412-15418.
[6] Y. Zhang, C. G. Fry, J. A. Pedersen, R. J. Hamers, *Anal. Chem.* **2017,** *89* (22), 12399-12407.
[7] G. Drisko, P.-F. Fazzini, A. Ibarra, S. Mourdikoudis, K. Fajerwerg, P. Fau, M. L. Kahn, *Nano Letters* **2018,** *18*, 1733−1738.
[8] Z. Pang, J. Zhang, W. Cao, X. Kong, X. Peng, *Nat. Commun.* **2019,** *10*, 2454.
[9] D. E. Jaskolska, D. F. Brougham, S. L. Warring, A. J. McQuillan, J. S. Rooney, K. C. Gordon, C. J. Meledandri, *Acs Appl. Nano Mater.* **2019,** *2* (4), 2230-2240.
[10] D. Doblas, T. Kister, M. Cano-Bonilla, L. Gonzalez-Garcia, T. Kraus, *Nano Lett.* **2019,** *19* (8), 5246-5252.
[11] Y. Champouret, G. Spataro, Y. Coppel, F. Gauffre, M. L. Kahn, *Nanoscale Adv.* **2020,** *2*, 1046-1053.
[12] A. Glaria, M. L. Kahn, B. Chaudret, P. Lecante, M. J. Casanove, B. Barbara, *Mater. Chem. Phys.* **2011,** *129* (1-2), 605-610.
[13] M. Dufour, J. Qu, C. Greboval, C. Methivier, E. Lhuillier, S. Ithurria, *Acs Nano* **2019,** *13* (5), 5326-5334.
[14] S. E. Crawford, M. J. Hartmann, J. E. Millstone, *Accounts Chem. Res.* **2019,** *52* (3), 695-703.
[15] G. Spataro, A. Dazzazi, S. Fortuny, Y. Champouret, Y. Coppel, J. Rubio-Garcia, A. Bouhaouss, F. Gauffre, M. L. Kahn, *Eur. J. Inorg. Chem.* **2016,** (13-14), 2056-2062.
[16] M. Ibanez, R. Hasler, A. Genc, Y. Liu, B. Kuster, M. Schuster, O. Dobrozhan, D. Cadavid, J. Arbiol, A. Cabot, M. V. Kovalenko, *J. Am. Chem. Soc.* **2019,** *141* (20), 8025-8029.
[17] S. Campisi, M. Schiavoni, C. E. Chan-Thaw, A. Villa, *Catalysts* **2016,** *6* (12), 185.
[18] T.-A. Chen, Y.-S. Shon, *Catalysts* **2018,** *8* (10), 428.
[19] S. T. Hunt, Y. Roman-Leshkov, *Accounts Chem. Res.* **2018,** *51* (5), 1054-1062.
[20] K. A. San, Y.-S. Shon, *Nanomaterials* **2018,** *8* (5), 346.

[21] Q. Tang, G. Hu, V. Fung, D.-E. Jiang, *Accounts Chem. Res.* **2018,** *51* (11), 2793-2802.
[22] M. D. Manning, A. L. Kwansa, T. Oweida, J. S. Peerless, A. Singh, Y. G. Yingling, *Biointerphases* **2018,** *13* (6), 06D502.
[23] I. Ojea-Jimenez, R. Capomaccio, I. Osorio, D. Mehn, G. Ceccone, R. Hussain, G. Siligardi, P. Colpo, F. Rossi, D. Gilliland, L. Calzolai, *Nanoscale* **2018,** *10* (21), 10173-10181.
[24] M. Wolska-Pietkiewicz, K. Tokarska, A. Grala, A. Wojewodzka, E. Chwojnowska, J. Grzonka, P. J. Cywinski, K. Kruczala, Z. Sojka, M. Chudy, J. Lewinski, *Chem. Eur. J.* **2018,** *24* (16), 4033-4042.
[25] Y. Iso, T. Isobe, *Ecs J. Solid State Sc.* **2018,** *7* (1), R3040-R3045.
[26] S. Mourdikoudis, L. M. Liz-Marzan, *Chem. Mater.* **2013,** *25* (9), 1465-1476.
[27] S. Tamang, C. Lincheneau, Y. Hermans, S. Jeong, P. Reiss, *Chem. Mater.* **2016,** *28* (8), 2491-2506.
[28] C. Amiens, B. Chaudret, D. Ciuculescu-Pradines, V. Colliere, K. Fajerwerg, P. Fau, M. Kahn, A. Maisonnat, K. Soulantica, K. Philippot, *New J. Chem.* **2013,** *37* (11), 3374-3401.
[29] B. ElRez, J.-P. Costes, C. Duhayon, L. Vendier, J.-P. Sutter, *Polyhedron* **2015,** *89*, 213-218.
[30] N. McCann, D. P., X. Wang, W. Conway, R. Burns, M. Attalla, G. Puxty, M. Maeder*J. Phys. Chem. A* **2009,** *113*, 5022-5029.
[31] M. Caplow, *J. Am. Chem. Soc.* **1968,** *90* (24), 6795-6803.
[32] D. B. Dell'Amico, F. Calderazzo, L. Labella, F. Marchetti, G. Pampaloni, *Chem. Rev.* **2003,** *103* (10), 3857–3898.
[33] M. Peters, B. Köhler, W. Kuckshinrichs, W. Leitner, P. Markewitz, T. E. Müller, *ChemSusChem* **2011,** *4* (9), 1216-1240.
[34] M. George, R. G. Weiss, *Langmuir* **2002,** *18* (19), 7124-7135.
[35] N. Belman, J. N. Israelachvili, Y. Li, C. R. Safinya, J. Bernstein, Y. Golan, *Nano Lett.* **2009,** *9* (5), 2088-2093.
[36] B. Luo, J. E. Rossini, W. L. Gladfelter, *Langmuir* **2009,** *25*, 13133-13141.
[37] T. Yu, R. Cristiano, R. G. Weiss, *Chem. Soc. Rev.* **2010,** *39* (5), 1435-1447.
[38] Y. Zhang, Y. Feng, J. Wang, S. He, Z. Guo, Z. Chu, C. A. Dreiss, *Chem. Commun.* **2013,** *49* (43), 4902-4904.
[39] C. Pages, Y. Coppel, M. L. Kahn, A. Maisonnat, B. Chaudret, *Chem. Phys. Chem.* **2009,** *10* (13), 2334-2344.
[40] M. L. Kahn, A. Glaria, C. Pages, M. Monge, L. Saint Macary, A. Maisonnat, B. Chaudret, *J. Mater. Chem.* **2009,** *19* (24), 4044-4060.
[41] G. Spataro, Y. Champouret, P. Florian, Y. Coppel, M. L. Kahn, *PCCP* **2018,** *20*, 12413 - 12421.
[42] C. Bonhomme, C. Gervais, D. Laurencin, *Prog. Nucl. Magn. Reson. Spect.* **2014,** *77*, 1-48.
[43] M. P. Hanrahan, Y. Chen, R. Blome-Fernández, J. L. Stein, G. F. Pach, M. A. S. Adamson, N. R. Neale, B. M. Cossairt, J. Vela, A. J. Rossini, *J. Am. Chem. Soc.* **2019,** *141*, 15532-15546.
[44] L. E. Marbella, J. E. Millstone, *Chem. Mater.* **2015,** *27*, 2721-2739.
[45] S. Mourdikoudis, R. M. Pallares, N. T. K. Thanh, *Nanoscale* **2018,** *10* (27), 12871-12934.
[46] A. G. M. Rankin, J. Trebosc, F. Pourpoint, J.-P. Amoureux, O. Lafon, *Solid State Nucl. Magn. Reson.* **2019,** *101*, 116-143.
[47] B. Zhang, B. Yan, *Anal. Bioanal. Chem* **2010,,** *396*, 973-982.
[48] Y. Champouret, Y. Coppel, M. L. Kahn, *J. Am. Chem. Soc.* **2016,** *138* (50), 16322-16328.
[49] D. Lee, M. Wolska-Pietkiewicz, S. Badoni, A. Grala, J. Lewiński, G. D. Paëpe, *Angew. Chem. Int. Ed.* **2019,** *58*, 17163-17168.
[50] M. Martínez-Prieto, B. Chaudret, *Acc. Chem. Res.* **2018,** *51*, 376-384.
[51] J. Zhang, H. Zhang, W. Cao, Z. Pang, J. Li, Y. Shu, C. Zhu, X. Kong, L. Wang, X. Peng, *J. Am. Chem. Soc.* **2019,** *141*, 15675-15683.
[52] J. Clauss, K. Schmidt-Rohr, A. Adam, C. Boeffel, H. W. Spiess, *Macromolecules* 1992, **25**, 5208

[53] B. B. Kharkov, V. I. Chizhik, S. V. Dvinskikh, *J. Phys. Chem. C* **2014,** *118*, 28308–13.
[54] M. L. Kahn, T. Cardinal, B. Bousquet, M. Monge, V. Jubera, B. Chaudret, *Chem. Phys. Chem.* **2006,** *7* (11), 2392-2397.
[55] N. McCann, D. Phan, X. Wang, W. Conway, R. Burns, M. Attalla, G. Puxty, M. Maeder, J. Phys. Chem. A, **2009**, 113 (17), 5022-29.
[56] Y. Coppel, G. Spataro, C. Pages, B. Chaudret, A. Maisonnat, M. L. Kahn, *Chem. Eur. J.* **2012,** *18* (17), 5384-5393.
[57] D. Massiot, F. Fayon, M. Capron, I. King, S. L. Calve, B. Alonso, J.-O. Durand, B. Bujoli, Z. Gan, G. Hoatson, *Magn. Res. Chem.* **2002,** *40*, 70-76.